

Article

Effects of Zn Addition and Twin Roll Casting Process on the Microstructure, Texture, and Mechanical Properties of the Mg-Al-Mn-Ca Sheet

Donghwan Eom ¹, Sangbong Yi ^{2,*}, Dietmar Letzig ² and No-Jin Park ^{1,*}

¹ School of Materials Science and Engineering, Kumoh National Institute of Technology, Gumi 39177, Republic of Korea; steins008@kumoh.ac.kr

² Institute of Material and Process Design, Helmholtz-Zentrum Hereon, Max-Planck-Str. 1, 21502 Geesthacht, Germany; dietmar.letzig@hereon.de

* Correspondence: sangbong.yi@hereon.de (S.Y.); njpark@kumoh.ac.kr (N.-J.P.)

Abstract: In this work, the microstructure and texture of Mg-1.0Al-xZn-0.2Mn-0.5Ca (wt.%, x = 0, 1) alloys, which were produced via conventional casting or twin roll casting (TRC), were investigated, and their relation to the mechanical properties of the sheets at the final gage was analyzed. In the Zn-containing AZMX1100 alloy sheets, the amount and size of the secondary phases were significantly reduced, in comparison to the Zn-free AMX100 alloy sheet. The TRC sheet shows a smaller grain structure and fine secondary phases in comparison to the sheets produced via the conventional casting process. The texture of the AMX100 sheet is characterized by the basal poles tilted in the sheet rolling direction (RD). In the AZMX1100 sheets, the texture with the tilted basal poles towards the RD and transverse direction (TD) was developed after recrystallization annealing, while the tilting angle of the basal pole in the TD is larger than in the RD. There is no significant difference in the texture between the sheets produced by the casting and TRC process. The highest yield strength was obtained in the AZMX1100 sheet produced by the TRC process, and all examined sheets showed the mechanical anisotropy in accordance with their textures.

Keywords: Mg alloy; twin roll casting; texture; microstructure; mechanical anisotropy



Citation: Eom, D.; Yi, S.; Letzig, D.; Park, N.-J. Effects of Zn Addition and Twin Roll Casting Process on the Microstructure, Texture, and Mechanical Properties of the Mg-Al-Mn-Ca Sheet. *Metals* **2024**, *14*, 261. <https://doi.org/10.3390/met14030261>

Academic Editors: Mariola Saternus and Ladislav Socha

Received: 17 January 2024

Revised: 16 February 2024

Accepted: 18 February 2024

Published: 22 February 2024



Copyright: © 2024 by the authors. Licensee MDPI, Basel, Switzerland. This article is an open access article distributed under the terms and conditions of the Creative Commons Attribution (CC BY) license (<https://creativecommons.org/licenses/by/4.0/>).

1. Introduction

In relation with the increasing global demands for carbon neutralization, the development of lightweight and environmentally friendly materials has drawn significant attention in transportation industries [1,2]. As the lightest structural metallic material, magnesium alloys have been widely investigated in the last decades. However, the commercial use of magnesium alloys is restricted because of their limited formability at low temperatures and strong tendency of forming a basal-type texture [3]. Due to the hexagonal close-packed (HCP) structure and limited number of active deformation modes, which cannot satisfy the Von Mises criterion of five independent slip systems for uniform plastic deformation, thermomechanical processes, such as rolling, extrusion, and forming operations, of magnesium alloys are carried out at an elevated temperature [4]. For this reason, the production of semi-final products of magnesium alloys needs a cost- and energy-intensive process. Thus, the research on magnesium alloys has surged to overcome the limitations through alloy and process improvement.

Magnesium sheets have traditionally been produced by the direct chill casting route, in which a thick slab machined from a casting billet is hot rolled to the final gage through a large number of rolling passes. Different to the conventional casting, the continuous casting combines solidification and rolling into a single step and saves a number of rolling and annealing steps. Twin roll casting (TRC), as a continuous casting process, fabricates a thin

strip with a thickness of 4–6 mm directly from the molten metal. In addition to the economic benefits achieved by reduced rolling steps and process cycle time, the combination of rapid solidification and deformation enables the production of the magnesium sheets with improved properties. For example, TRC strips have an already refined microstructure, fine intermetallic particles, and high solubility based on a fast cooling rate, such that the sheets in the final gage have fine intermetallic phases and a homogeneous grain microstructure [5]. However, commonly occurring defects formed during TRC include centerline segregation and inverse segregation. The centerline segregation arises from the strip formation mechanism where two solidification fronts having a relatively high chemical segregation meet at the mid-thickness area. On the other hand, the inverse segregation is generated when the remaining melt with a higher solute concentration is squeezed out by the rolling force through the boundaries of columnar grains towards the strip surface. Such microstructure inhomogeneity developed during TRC can be diminished by an appropriate alloy composition, TRC process conditions, and post-TRC treatments [6]. With regard to the development of highly formable magnesium alloy sheets, it is essential to control the crystallographic texture being favorable for the activation of the dislocation slip. The formation of a strong basal-type texture, in which most grains have their *c*-axes in the sheet normal direction (ND), causes a significant ductility reduction due to the restricted activity of *a* dislocation slip, especially during the deformation along ND. Even though the strain along the ND of a sheet having a strong basal-type texture can be accommodated by the activation of a non-basal slip, e.g., pyramidal *c+a* slip with a Burgers vector of $\langle 11\text{--}23 \rangle$, their activities are in general limited because of the high critical resolved shear stress (CRSS) at a low temperature. By weakening the texture intensity and altering the basal-type texture to a wide spread of basal poles away from the ND, the room temperature formability can be significantly improved. The addition of rare earth elements (RE) or Ca has been acknowledged as an effective way to suppress the formation of a strong basal-type texture during the thermomechanical treatments of Mg alloys. Indeed, the sheets with the weakened texture show an improved formability [1,7]. Even though the alloying of RE largely weakens the texture in semi-finished products, a number of studies have committed to define RE-free alloys with a weakened forming tendency of a basal-type texture, because of the unstable supply chains and environmental issues. The AZMX (Mg-Al-Zn-Mn-Ca) base alloys, which do not contain RE, have been developed as a highly formable sheet alloy. The Zn addition into the Mg-Al-Ca alloy induces the weak texture formation with a non-basal texture component, like basal poles split towards the sheet rolling (RD) and transverse direction (TD) simultaneously [8–14].

The present study aims to investigate the influence of the sheet processes on the microstructure and mechanical properties of the Mg-1.0Al-1.0Zn-0.2Mn-0.5Ca alloy. Special emphasis has been given on the comparison between the sheets produced via TRC and conventional casting processes. Moreover, the role of Zn addition on the microstructure and texture development has been investigated by a comparative study of the Mg-1.0Al-0.2Mn-0.5Ca and Mg-1.0Al-1.0Zn-0.2Mn-0.5Ca sheets produced by DC casting and conventional hot rolling processes.

2. Materials and Methods

The ingots of the AMX100 and AZMX1100 alloys, with the nominal compositions of Mg-1Al-0.2Mn-0.5Ca and Mg-1Al-1Zn-0.2Mn-0.5Ca in wt.%, were cast at 730 °C into a steel mold with the dimension of 150 (w) × 195 (h) × 40 (t) mm under a Ar and CO₂ atmosphere. The steel mold was preheated to 250 °C before pouring the molten metal, to reduce the casting defects. The rolling slabs with 85 (w) × 4.8 (t) mm were machined from the cast blocks. To investigate the difference between the sheets produced via DC casting and continuous casting, a strip of the AZMX1100 alloy with a thickness of 4.8 mm and width of 150 mm was produced via TRC at a melt temperature of 730 °C and rolling speed of 2.36 m/min. The TRC facility (lab-scale continuous caster, Daham ENC) used in the present study is equipped with an electric melting furnace with a maximum capacity of

15 kg of magnesium alloys and rolling mills with a diameter of 250 mm and water cooling units. The rolling slabs machined from the cast blocks and the TRC strip, which have the same initial thickness of 4.8 mm, were rolled to the final gage of 1 mm. The hot rolling was carried out at 410 °C with a pass reduction degree of 18%, to the total rolling reduction of 79%. To avoid cracking during the rolling, intermediate annealing was conducted at the rolling temperature for 30 min after each rolling step. The recrystallization annealing of the rolled sheets was performed at 350 °C for 120 min and air cooled. The experimental conditions to produce the sheets are summarized in Table 1.

Table 1. Casting and rolling conditions to produce the sheets examined in the present study.

| Alloy | Nominal Composition (wt.%) | Casting Method | Rolling | Recrystallization Annealing |
|------------------|----------------------------|-------------------|---|--|
| Casting AMX100 | Mg-1Al-0.2Mn-0.5Ca | DC casting | Hot rolling at 410 °C, total reduction 79% (common to all alloys) | 350 °C for 120 min (common to all alloys) |
| Casting AZMX1100 | Mg-1Al-1Zn-0.2Mn-0.5Ca | DC casting | | |
| TRC AZMX1100 | Mg-1Al-1Zn-0.2Mn-0.5Ca | Twin roll casting | | |

Metallographic examination was conducted by optical microscopy on the TD-RD plane as well as on the ND-RD plane. It is to mention that the microstructural features, e.g., average grain size and distribution of secondary phases, are quite similar on the TD-RD and ND-RD planes. For the optical microstructure observation, the samples were ground with emery paper to grit 4000 and mechanically polished with 0.3 µm of diamond paste, which was followed by the etching using picric acid-based solution (100 mL of distilled water, 100 mL of ethanol, 6 mL of acetic acid, 1.6 g of picric acid) to reveal the microstructural features. The chemical compositions and distribution of the secondary phases were analyzed by EDS equipped on a scanning electron microscopy (SNE-4500MTM, SEC, Suwon, Republic of Korea). The average grain size of the rolled and annealed samples was determined by the linear intercept method of the micrographs on the TD-RD plane. Mechanical properties were examined by tensile tests using the samples prepared along the RD and TD with 25 mm in gage length and 6 mm in width, corresponding to the ASTM E8M subsize tensile sample, at room temperature and the initial strain rate of $1.0 \times 10^{-3} \text{ s}^{-1}$ using a universal testing machine (MINOS-100TM, MTDI, Daejeon, Rep. of Korea). The global texture of the rolled and recrystallized sheets was measured on the TD-RD plane using an X-ray diffraction (XPert ProTM, Pananalytical, Almelo, The Netherlands, at 40 kV, 40 mA). The sheet samples for the texture measurements were mechanically ground and polished approximately to the mid-thickness. Six pole figures, $\{1\ 0\ -1\ 0\}$, $\{0\ 0\ 0\ 1\}$, $\{1\ 0\ -1\ 1\}$, $\{1\ 0\ -1\ 2\}$, $\{1\ 1\ -2\ 0\}$, and $\{1\ 0\ -1\ 3\}$, were measured up to a tilt angle of 70°/5°. The orientation distribution function (ODF) and complete pole figures were calculated using a Matlab-based toolbox MTEX [15]. In the present study, the recalculated $\{0\ 0\ 0\ 1\}$ pole figures are used to present the global texture.

3. Results and Discussion

Figure 1 presents the optical micrographs of the casting blocks of AMX100 and AZMX1100 alloys. Both ingots show relatively large grains with an average size of 120 µm and spherical secondary phases. The AMX100 alloy has a larger amount of secondary phases in comparison to the AZXM1100 alloy, with the area fraction of 7% and 1%, respectively. The microstructure of the TRC strip of the AZXM1100 alloy, Figure 2a, is characterized by the globular grains at the central area, Figure 2b, and the columnar grains at the surface area, Figure 2c. Because the solidification concurrently occurs with the rolling deformation, the columnar grains at the near-surface area show an inclination in the RD. The centerline segregation and inverse segregation near the surface of the strip, which result from the solidification of the remaining melt and the squeezing of the melt through the solid–liquid interface due to the rolling force during the TRC process, respectively, are marked by white rectangles. Such microstructural features, i.e., columnar grains at the near-surface and a relatively large area of the globular grains at the mid-thickness, observed in

the TRC strip indicate that the solidification completes after passing the rolling deformation zone, which results from a relatively high rolling speed during the TRC process. It is also mentioned that casting defects, like voids and inclusions, are observed in both cast blocks and the TRC strip. Even though there are no micropores observed in both ingots, there would be microporosity due to the shrinkage with local inhomogeneity in chemical compositions, e.g., at grain boundaries. Figure 3 shows the SEM images of the TRC strip and the chemical compositions analyzed by EDS. The dendrite structures decorated with the segregation and the fine secondary phases along the boundaries are clearly visible in Figure 3a. The secondary phase particles formed at the boundaries of columnar grains and at the centerline segregation are mainly composed of eutectic lamellae, and they are much coarser, with a length of some tens to some hundreds of micrometers, than that formed at the dendrite boundaries, Figure 3b,c. The chemical composition of the TRC plate was examined by EDS analysis on the area covering some columnar grains, and it matches to the nominal composition, Figure 3a. The coarse secondary phases at the columnar grains and at the centerline segregation show a high concentration of all alloying elements, except Mn. Such microstructural inhomogeneity should be eliminated by subsequent thermomechanical treatments, e.g., homogenization, hot rolling, and annealing treatments. A previous study showed that the centerline segregation in a TRC strip of AZX310 alloy, with some mm in length and 80 μm in thickness, can be fragmented to agglomerates of the small spheroidal particles with 0.5–1 μm in diameter by the post-TRC thermomechanical treatments [16]. While the coarse eutectic lamellae in the TRC strip can lead to premature failure, the fine spheroidal particles fragmented from the centerline segregation can act as a strengthener. In this regard, the low alloying amount in the examined alloy is obviously conducive to obtain a homogeneous microstructure.

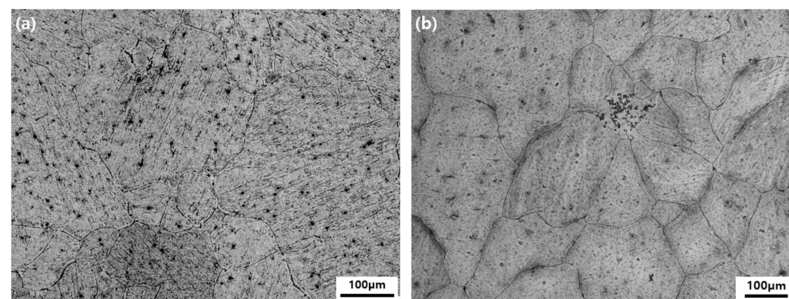


Figure 1. Optical micrographs of the cast blocks of (a) AMX100 and (b) AZMX1100 alloy.

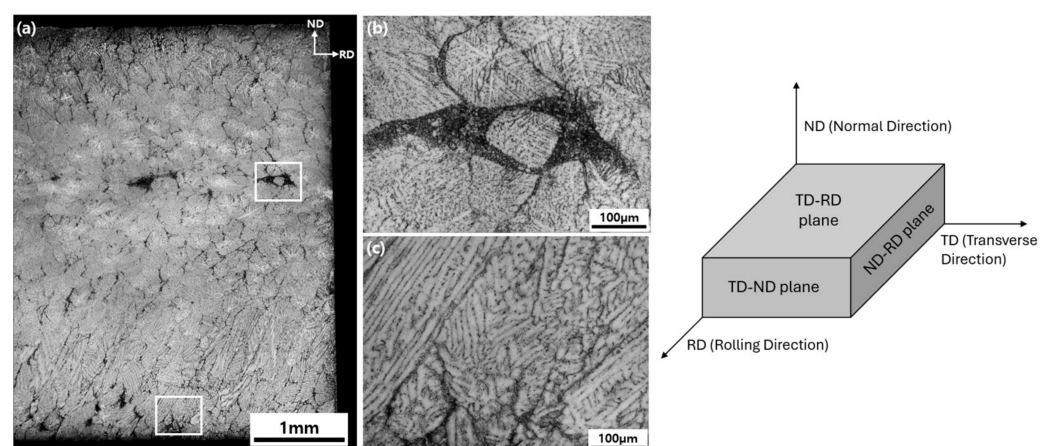


Figure 2. Optical micrographs of the as-TRC strip of the AZMX1100 alloy with a thickness of 4.8 mm at the (a) ND-RD plane, (b) centerline segregation, and (c) columnar structure inclined in the RD at the near-surface area. The sample directions and planes are schematically shown.

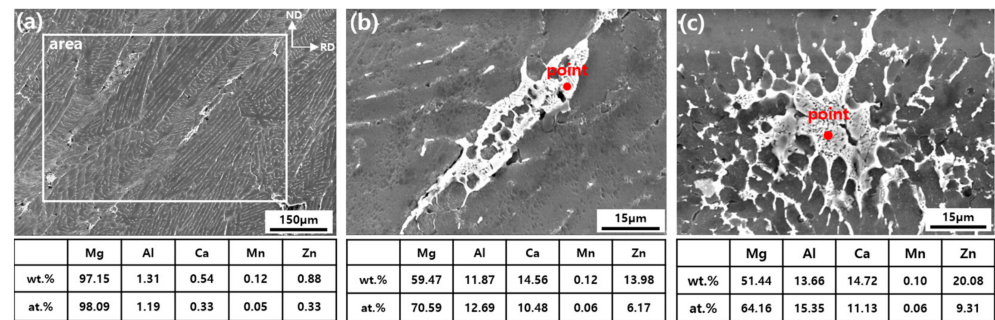


Figure 3. SEM images of the as-TRC strip of the AZMX1100 alloy at the (a) ND-RD plane, (b) secondary phase particle formed at the boundary of columnar grains, (c) secondary phase particle formed at the centerline segregation. EDS results analyzed on the rectangular area marked on (a), and the secondary phases marked on (b,c) are listed in the tables.

Figure 4 shows the optical micrographs of the hot-rolled sheets and the annealed sheets at 350 °C for 120 min. The as-rolled sheets, Figure 4a–c, have a globular grain structure with a similar average grain size of 12–13 μm. The globular grain morphology of the as-rolled sheets is attributed to the intermediate annealing. The secondary phases appearing dark in the optical micrograph of the AMX100 sheet are relatively large and they align parallel to the RD, while such secondary phases aligned in the RD are not found in other sheets. After the heat treatment, Figure 4d–f, the AZXM1100 sheet produced via TRC (named TRC sheet, hereinafter) exhibits finer grains than the sheets from the ingot casting (named casting sheets).

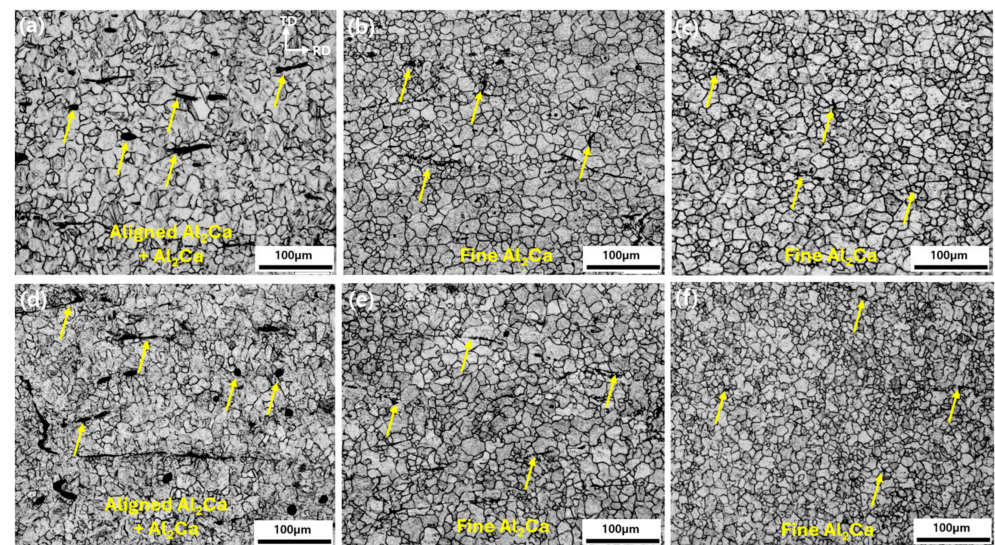


Figure 4. Optical micrographs of the hot-rolled sheets of (a) casting AMX100, (b) casting AZMX1100, (c) TRC AZMX1100 alloys, and after the heat treatment at 350 °C for 2 h of (d) casting AMX100, (e) casting AZMX1100, and (f) TRC AZMX1100 sheets. The arrows indicate the secondary phases.

Figure 5 displays the frequency distribution plot of grain size, which was analyzed by the linear intercept method. While the as-rolled sheets have a similar grain size of about 13 μm, the annealed ones show a difference in the grain size. The annealed sheets have a finer grain size than the as-rolled sheets, which indicates that the new grains were formed during the heat treatment. The annealed TRC AZXM1100 sheet shows the smallest grain size of 8.4 μm. In addition, the TRC AZXM1100 sheet displays a narrower grain size distribution with a steeper distribution peak, which indicates a more homogeneous microstructure in terms of the grain size. The fine and homogeneous grain structure of the TRC sheet is attributed to the faster solidification rate during the TRC process, in

comparison to the conventional casting process. The rapid cooling leads to the alloying elements remaining trapped in the matrix as solute elements, rather than contributing to forming secondary phases. The solute atoms restrict the grain growth due to the solute pinning effects, resulting in finer grain sizes. The EDX analysis was conducted to reveal the chemical compositions of the secondary phases in the annealed sheets. The stringers in the casting sheets predominantly contain Al and Ca, and the atomic ratio appears to be approximately 2:1, Figure 6. These results suggest that the thin linear secondary phases are the Al_2Ca phase, which is supported by the phase diagram in Figure 7. In the AMX100 casting sheet, the thin linear secondary phases are formed continuously over many grains, while those in the AZXM1100 sheets are discontinuous. The average length of the linear Al_2Ca phases is 10 μm and 2.3 μm in the AMX100 and AZXM1100 casting sheet, respectively. The TRC sheet does not contain such line-shaped phases, and the average size of the observed secondary phases is 0.6 μm . The small spheroidal phases formed in the matrix grains of the AZXM1100 casting sheet appear to be Al-Mn phases, as shown in the EDX mapping result, indicating a relatively higher Mn concentration at the corresponding sites, Figure 6d. These results imply that the Zn addition contributes to the refinement and reduced amount of the Al_2Ca phases, also by the formation of the Zn- and Ca- containing phases, e.g., $\text{Mg}_5\text{Zn}_5\text{Ca}_2$. The TRC process accompanying with very rapid solidification results in the alloying elements being incorporated within the matrix rather than contributing to the formation of secondary phases, such that the AZMX1100 TRC sheet has the smallest amount of secondary phases.

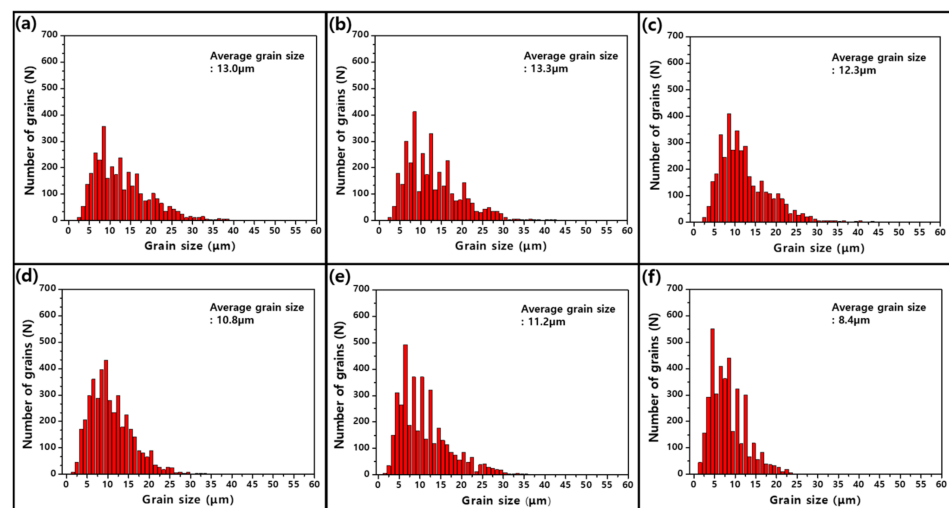


Figure 5. Grain size distribution graph of the as-rolled sheets of (a) casting AMX100, (b) casting AZMX1100, (c) TRC AZMX1100, and after the heat treatment at 350 °C for 2 h of (d) casting AMX100, (e) casting AZMX1100, and (f) TRC AZMX1100 sheets.

The crystallographic texture of the examined sheets is demonstrated in Figure 8. The as-rolled sheets show the splitting basal poles towards the RD, with a relatively low max 0001 pole density of 3.9 and 4.6 m.r.d. (multiples of a random distribution), in comparison to the conventionally available Mg alloy sheets. While the AMX100 sheet shows the 0001 pole split into the RD, the Zn-containing AZMX1100 sheets form an additional 0001 pole split into the TD. It is noteworthy that a commercial AZ31 sheet shows a strong basal-type texture, with a max pole density higher than 10 m.r.d. and a basal pole spread into RD [17,18]. The annealing of the rolled sheets at 350 °C results in a texture weakening that accompanies with the large split of 0001 poles into the TD in the AZMX1100 sheets. The annealed casting and TRC AZMX1100 sheets have the lowest texture intensity, with a pole density of 2.9 m.r.d. Such texture change results from that the basal pole split into the RD preferentially diminishes, while the basal poles splitting into the TD retain their intensity during the annealing. The texture weakening concurrently occurring with the

formation of the TD split of the basal poles has been reported in Mg alloy sheets containing RE and Zn simultaneously [19–21]. Y.M. Kim et al. [20] reported that the development of the characteristic texture in the Mg-Zn-Y alloy is attributed to the solute segregation along the stacking faults on the (0001) plane and impeded grain growth, resulting in a restricted growth in the [0001] direction. In addition, the solute segregation at grain boundaries has been reported in relation to the texture weakening. Zeng et al. [22] compared the microstructure and texture evolution between the binary and ternary alloys, i.e., Mg-0.4Zn, Mg-0.1Ca, and Mg-0.3Zn-0.1Ca. It was shown that the grain boundary migration is more effectively hindered in the ternary alloy, which leads to a weaker texture in the fully recrystallized condition. The authors inferred that the boundary energy can be more effectively reduced by the co-segregation of Zn and Ca, in comparison to the binary alloys. The previous studies support the present results suggesting that the Zn addition is the main contributor to developing the weak texture with the basal poles splitting in the TD. It is notable that there is no significant difference in the texture between the AZMX1100 sheets produced via casting and the TRC processes.

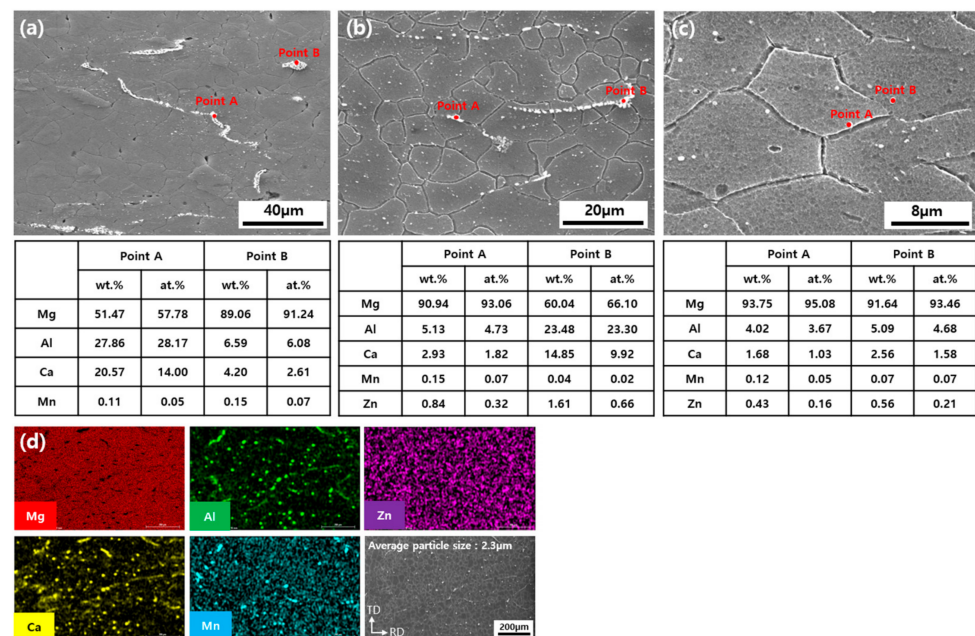


Figure 6. SEM images of the hot-rolled sheets of (a) casting AMX100, (b) casting AZMX1100, (c) TRC AZMX1100 alloys. EDS results analyzed on the secondary phases found in the rolled sheets are listed in the table. EDS area mapping data of the hot-rolled sheets of (d) casting AZMX1100. (Different magnifications were employed due to the large differences in size of the secondary phases between the sheets).

Figure 9 displays the stress–strain curves of the annealed sheets examined in the RD and TD at room temperature, and the tensile properties are listed in Table 2. The AMX100 casting sheet shows a lower yield strength (YS) in the RD than that in the TD, 137 MPa and 148 MPa, respectively. The texture of the AMX100 sheet shows the basal poles tilted in the RD, which promotes the basal $\langle a \rangle$ slip in the RD due to a high Schmid factor and results in a lower YS. In the case of the AZMX1100 sheets, the tilting angle of the basal pole in the TD is larger than that in the RD, which corresponds to a higher Schmid factor for the basal $\langle a \rangle$ slip in the TD. Thus, the AZMX1100 sheets have a lower YS in the TD. The higher YS of the AZMX1100 sheets, in comparison to that of the AMX100, can be understood as a result of solute strengthening. As shown in Figures 4 and 6, the AMX100 sheet shows the long extended Al_2Ca phases, while the AZMX1100 sheets have a large amount of relatively finer particles. In addition to the effective solute strengthening in the AZMX1100 sheets, which can be deduced from the absence of the long-extended particles,

the finer secondary phases bring about precipitation strengthening [23]. Moreover, the fine grain structure and the higher amount of the solute resulting from the rapid solidification of the TRC AZMX1100 sheet should lead to the highest YS (and UTS) within the examined alloys, 174 MPa (250 MPa) and 151 MPa (244 MPa) in the RD and TD, respectively. The higher fracture strain (ϵ_f) is observed in the sheet planar direction of the lower YS, i.e., in the direction corresponding to the larger tilt of the 0001 pole, i.e., RD of the casting AMX100 and TD of the AZMX1100 sheets. It is hypothesized that the higher activity of the basal slip, based on the texture and the higher Schmid factor, yields an improvement in ductility.

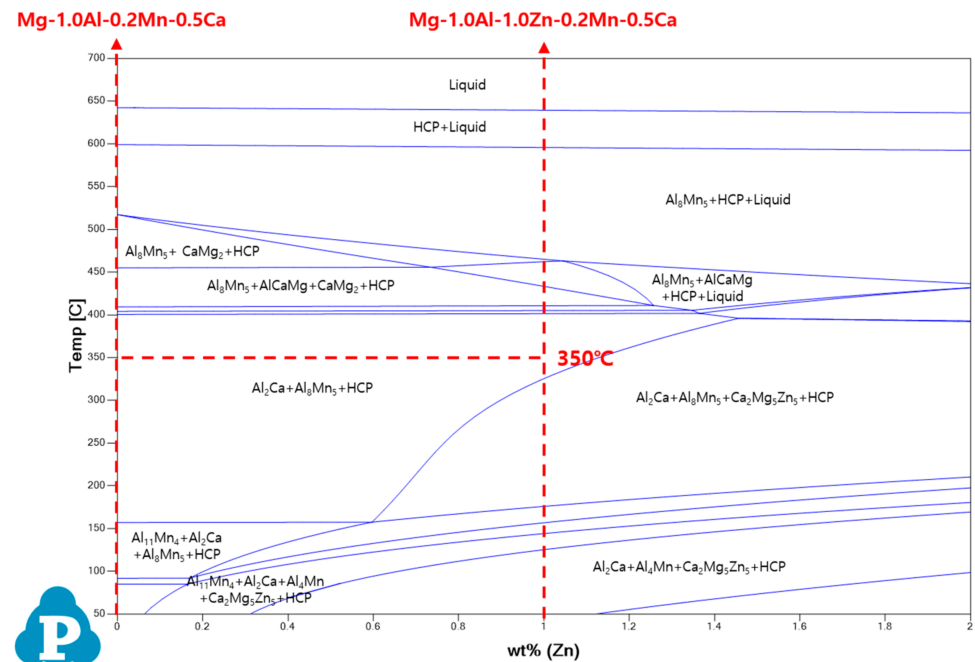


Figure 7. Phase diagram of Mg-1.0Al-(0~1)Zn-0.2Mn-0.5Ca, in wt.%, calculated using thermodynamic simulation software Pandat (<https://computherm.com/software>, accessed on 17 February 2024) with PanMg_TH (CompuTherm LLC, Middleton, WI, USA).

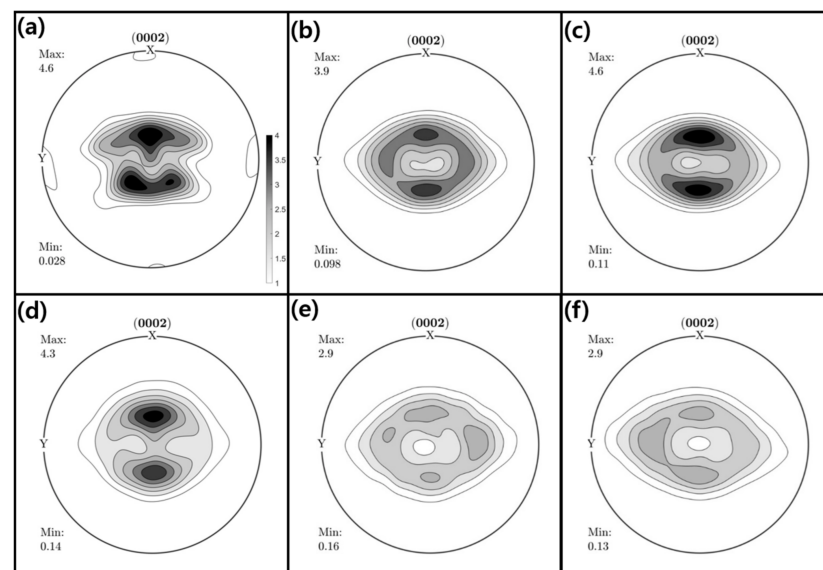


Figure 8. Recalculated (0002) pole figures of the hot-rolled sheets of (a) casting AMX100, (b) casting AZMX1100, (c) TRC AZMX1100 alloys, and the rolled sheet after the heat treatment at 350 °C for 2 h at (d) casting AMX100, (e) casting AZMX1100, and (f) TRC AZMX1100 (Maximum and minimum pole density in multiples of random distribution, m.r.d., X: RD, Y: TD).

Table 2. Tensile properties at room temperature of the examined sheets after annealing at 350 °C for 2 h (average values from three tests are given in the table).

| Process | Alloy | RD | | | TD | | |
|---------|----------|----------|-----------|------------------|----------|-----------|------------------|
| | | YS (MPa) | UTS (MPa) | ϵ_f (%) | YS (MPa) | UTS (MPa) | ϵ_f (%) |
| Casting | AMX100 | 137 ± 3 | 216 ± 3 | 21.1 ± 2.5 | 148 ± 3 | 214 ± 3 | 18.2 ± 2.9 |
| | AZMX1100 | 153 ± 3 | 237 ± 2 | 22.9 ± 1.3 | 130 ± 4 | 234 ± 4 | 26.9 ± 1.1 |
| TRC | AZMX1100 | 174 ± 3 | 250 ± 2 | 20.5 ± 1.1 | 151 ± 3 | 244 ± 3 | 23.6 ± 1.2 |

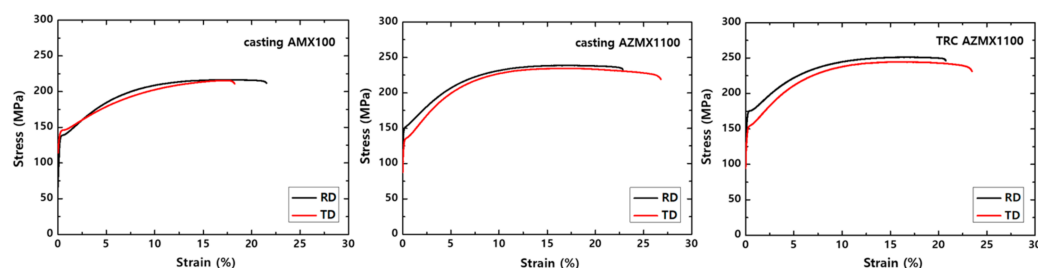


Figure 9. Stress–strain curves of the sheets after the heat treatment at 350 °C for 2 h.

4. Conclusions

Mg-1.0Al-0.2Mn-0.5Ca (AMX100) and Mg-1.0Al-1.0Zn-0.2Mn-0.5Ca (AZMX1100) alloy sheets were produced via DC casting or the TRC process. The effects of process differences and Zn addition on the microstructure, texture, and mechanical properties of sheets were analyzed and the following conclusions were drawn:

1. In the TRC AZMX1100 sheet, a columnar structure inclined along the rolling direction and centerline segregation was observed, while a coarse grain structure with about 120 μm in average size was formed in the DC cast block. A higher fraction of the second phase was formed in the AMX100 alloy than in the AZMX1100 alloy sheets.
2. The TRC AZMX1100 sheet showed the finest grain structure with an average grain size of 8.4 μm , which results from the alloying elements dissolving in the matrix as solid solution at a higher concentration due to the fast cooling rate of the TRC process. The casting AZMX1100 and casting AMX100 sheets show a similar grain size of approximately 11.0 μm . However, a relatively coarse grain structure with a large number of Al_2Ca phases is formed in the AMX100 sheet.
3. In all the sheets examined in this study, a weak texture with the basal pole spread in the RD or TD was developed. The texture was further weakened by the subsequent heat treatment. The Zn-containing TRC AZMX1100 and casting AZMX1100 sheets showed the basal poles largely tilted in the TD, independent of the process.
4. The high YS of the casting AZMX1100 sheet was brought about by the strengthening by the solid solution and fine precipitates, while the highest YS of 174 MPa of the TRC AZMX1100 sheet is additionally attributed to the finer grain size. The planar anisotropy in the yield strength can be understood from the texture of the sheets. For example, the lower YS in the RD of the AMX100 sheet results from the basal poles tilted in the RD, while the lower YS in the TD of the AZMX1100 sheet is associated with the basal poles largely tilted in the TD.

Author Contributions: Conceptualization, N.-J.P. and S.Y.; Experiments and analysis of the experimental results, D.E.; Writing—original draft preparation, D.E. and S.Y.; Writing—review and editing, D.E., S.Y., D.L. and N.-J.P.; Project administration, N.-J.P. and D.L. All authors have read and agreed to the published version of the manuscript.

Funding: This research received no external funding.

Data Availability Statement: The raw data supporting the conclusions of this article will be made available by the authors on request.

Acknowledgments: The authors are grateful to Y.H. Go at the Korea Institute of Materials Science (KIMS) and Y.K. Shin at Helmholtz-Zentrum hereon (Hereon) for supporting the twin roll casting process of the initial materials, sample preparation, and EBSD analysis.

Conflicts of Interest: The authors declare no conflicts of interest.

References

1. Chaudry, U.M.; Tekumalla, S.; Gupta, M.; Jun, T.S.; Hamad, K. Designing highly ductile magnesium alloys: Current status and future challenges. *Crit. Rev. Solid State Mater. Sci.* **2021**, *47*, 194–281. [[CrossRef](#)]
2. Joost, W.J.; Krajewski, P.E. Towards magnesium alloys for high-volume automotive applications. *Scr. Mater.* **2017**, *128*, 107–112. [[CrossRef](#)]
3. Kim, N.J. Magnesium sheet alloys: Viable alternatives to steels. *Mater. Sci. Technol.* **2014**, *30*, 1925–1928. [[CrossRef](#)]
4. Nie, J.F.; Shin, K.S.; Zeng, Z.R. Microstructure, Deformation, and Property of Wrought Magnesium Alloys. *Metall. Mater. Trans. A* **2020**, *51*, 6045–6109. [[CrossRef](#)]
5. Javaid, A.; Czerwinski, F. Progress in twin roll casting of magnesium alloys: A review. *J. Alloys Compd.* **2021**, *9*, 362–391. [[CrossRef](#)]
6. Park, S.S.; Park, W.J.; Kim, C.H. The Twin-Roll Casting of Magnesium Alloys. *JOM* **2009**, *61*, 14–18. [[CrossRef](#)]
7. Cai, Z.X.; Jiang, H.T.; Tang, D.; Ma, Z.; Kang, Q. Texture and stretch formability of rolled Mg-Zn-RE (Y, Ce, and Gd) alloys at room temperature. *Rare Met.* **2013**, *32*, 441–447. [[CrossRef](#)]
8. Zhao, L.Q.; Wang, C.; Chen, J.C.; Ning, H.; Yang, Z.Z.; Xu, J.; Wang, H.Y. Development of weak-textured and high-performance Mg-Zn-Ca alloy sheets based on Zn content optimization. *J. Alloys Compd.* **2020**, *849*, 156640. [[CrossRef](#)]
9. Nakata, T.; Xu, C.; Suzawa, K.; Yoshida, K.; Kawabe, N.; Kamado, S. Enhancing mechanical properties of rolled Mg-Al-Ca-Mn alloy sheet by Zn addition. *Mater. Sci. Eng. A* **2018**, *737*, 223–229. [[CrossRef](#)]
10. Li, Z.H.; Sasaki, T.T.; Bian, M.Z.; Nakata, T.; Yoshida, Y.; Kawabe, N.; Kamado, S.; Hono, K. Role of Zn on the room temperature formability and strength in Mg-Al-Ca-Mn sheet alloys. *J. Alloys Compd.* **2020**, *847*, 156347. [[CrossRef](#)]
11. Bian, M.Z.; Sasaki, T.T.; Nakata, T.; Yoshida, Y.; Kawabe, N.; Kamado, S.; Hono, K. Bake-hardenable Mg-Al-Zn-Mn-Ca sheet alloy processed by twin-roll casting. *Acta Mater.* **2018**, *158*, 278–288. [[CrossRef](#)]
12. Trang, T.; Zhang, J.; Kim, J.H.; Zargarani, A.; Hwang, J.K.; Suh, B.I.; Kim, N.J. Designing a magnesium alloy with high strength and high formability. *Nat. Commun.* **2018**, *9*, 2522. [[CrossRef](#)] [[PubMed](#)]
13. Bian, M.Z.; Sasaki, T.T.; Nakata, T.; Kamado, S.; Hono, K. Effects of rolling conditions on the microstructure and mechanical properties in a Mg-Al-Ca-Mn-Zn alloy sheet. *Mater. Sci. Eng. A* **2018**, *730*, 147–154. [[CrossRef](#)]
14. Wang, Q.; Jiang, B.; Tang, A.; Fu, J.; Jiang, Z.; Sheng, H.; Zhang, D.; Huang, D.; Pan, F. Unveiling annealing texture formation and static recrystallization kinetics of hot-rolled Mg-Al-Zn-Mn-Ca alloy. *Mater. Sci. Technol.* **2020**, *43*, 104–118. [[CrossRef](#)]
15. Hielscher, R.; Schaeben, H. A novel pole figure inversion method: Specification of the MTEX algorithm. *Appl. Crystallogr.* **2008**, *41*, 1024–1037. [[CrossRef](#)]
16. Yi, S.; Park, J.H.; Letzig, D.; Kwon, O.D.; Kainer, K.U.; Kim, J.J. *Magnesium Technology 2016*; Singh, A., Solanki, K., Manuel, M.V., Neelameggham, N.R., Eds.; The Minerals, Metals & Materials Society: Cham, Switzerland, 2016; pp. 383–387.
17. Steiner, M.A.; Bhattacharyya, J.J.; Agnew, S.R. The origin and enhancement of {0001}<11–20> texture during heat treatment of rolled AZ31B magnesium alloys. *Acta Mater.* **2015**, *95*, 443–455.
18. Jia, X.P.; Hu, X.D.; Zhao, H.Y.; Ju, D.Y.; Chen, D.L. Texture evolution of AZ31 magnesium alloy sheets during warm rolling. *J. Alloys Compd.* **2015**, *645*, 70–77. [[CrossRef](#)]
19. Mouhib, F.; Pei, R.; Erol, B.; Sheng, F.; Kerzel, S.K.; Samman, T.A. Synergistic effects of solutes on active deformation modes, grain boundary segregation and texture evolution in Mg-Gd-Zn alloys. *Mater. Sci. Eng. A* **2022**, *847*, 143348. [[CrossRef](#)]
20. Kim, Y.M.; Mendis, C.; Sasaki, T.; Letzig, D.; Pyczak, F.; Hono, K.; Yi, S.B. Static recrystallization behaviour of cold rolled Mg-Zn-Y alloy and role of solute segregation in microstructure evolution. *Scr. Mater.* **2017**, *136*, 41–45. [[CrossRef](#)]
21. Hoseini-Athar, M.M.; Mahmudi, R.; Babu, R.P.; Hedstrom, P. Microstructure, texture, and strain-hardening behavior of extruded Mg-Gd-Zn alloys. *Mater. Sci. Eng. A* **2020**, *772*, 138833. [[CrossRef](#)]
22. Zeng, Z.R.; Zhu, Y.M.; Xu, S.W.; Bian, M.Z.; Davies, C.H.J.; Birbilis, N.; Nie, J.F. Texture evolution during static recrystallization of cold-rolled magnesium alloys. *Acta Mater.* **2016**, *105*, 479–494. [[CrossRef](#)]
23. Jiang, Z.; Jiang, B.; Yang, H.; Yang, Q.; Dai, J.; Pan, F. Influence of the Al₂Ca phase on microstructure and mechanical properties of Mg-Al-Ca alloys. *J. Alloys Compd.* **2015**, *647*, 357–363. [[CrossRef](#)]

Disclaimer/Publisher’s Note: The statements, opinions and data contained in all publications are solely those of the individual author(s) and contributor(s) and not of MDPI and/or the editor(s). MDPI and/or the editor(s) disclaim responsibility for any injury to people or property resulting from any ideas, methods, instructions or products referred to in the content.